Preparation, characterisation, drug loading and release properties of a novel KIT-6/poly(AA-EGDMA) nanocomposite

Anahita Shafiei[1], *S. Yahya*[1], *Sh. Beheshtiha*[1], *Majid M. Heravi*[1] ✉, *Roozbeh Javad Kalbasi*[2]

[1]*Department of Chemistry, Alzahra University, Vanak, Tehran, Iran*
[2]*Faculty of Chemistry, Kharazmi University, Tehran, Iran*
✉ *E-mail: mmheravi@alzahra.ac.ir*

Published in Micro & Nano Letters; Received on 22nd June 2017; Revised on 4th August 2017; Accepted on 1st September 2017

A KIT-6/poly(acrylic acid-ethylene glycol dimethacrylate) (KIT-6/Poly(AA-EGDMA) nanocomposite was synthesised as an adequate carrier. KIT-6 as a three-dimensional cubic symmetric structure was prepared by the sol–gel method. Polymerisation was carried out through the in situ method in which EGDMA was cross-linked by AA inside KIT-6 pores. This mesostructure acts as a smart uptake and release of the ibuprofen (IBU) system. Diverse characterisation techniques including Fourier transform infrared spectroscopy, X-ray powder diffraction, Brunauer–Emmett–Teller, thermal gravimetric, scanning electron microscopy and ultraviolet-visible spectroscopy were employed to determine the relationship between the carrier nature and drug release performance. The KIT-6/Poly(AA-EGDMA) was modified by changing the ratio of the polymer and IBU as well as its time-loading. The results proved that the KIT-6/Poly(AA-EGDMA) has the ability of drug adsorption and slow release in a simulated body fluid.

1. Introduction: Nowadays, design and preparation of materials for harmless and efficient drug delivery have attracted enormous consideration and stimulated the interest of bioorganic chemists by playing a principal role in modern medicine [1]. To increase drug efficiency and decrease the unwanted opposing side effects, the degradation of its therapeutic characteristics should be avoided and its delivery rate must be controlled. In this way, the drug would be more patient-amenable leading to its commercial importance and value [2].

In recent years, several nanoparticle-based drug delivery systems (DDSs), i.e. as dendrimers, liposomes, polymeric micelle and different inorganic nanoparticles have been prepared and introduced. They have been amended to increase the effectiveness and diminish the systemic toxicity of various drugs, particularly those known as anti-cancer drugs [2–6]. Among these inorganic nanoparticles, a mesoporous silica nanoparticle (MSN) has attracted enormous interest due to its outstanding features. MSNs have been found to show superb qualities including high pore volume, large surface area, available surface functionalisation and conspicuous biocompatibility [7–11]. Moreover, MSNs have been modified in order to act as stimuli-responsive controlled release systems. Due to their exceptional structures, MSNs could be utilised as selective host–guest molecules bearing different functionalities, sizes, shapes as well as DNAs, drugs, genes and proteins [12].

In comparison with the most common organic carriers, MSNs show the substantial merit of being free from different biochemical attacks and bioerosion; nevertheless, the loading bioactive molecule ruptures are released in MSNs, and cannot be released in a well-controlled fashion to accurately and specifically match the actual physiological requirements at an appropriate time/site. Due to these drawbacks, the applications of unmodified MSNs are limited and their modification, especially in the nanosize, is in much demand. Each successful attempt may lead to the discovery of a novel drug nanocarrier [13].

To unravel the problem and prepare modified MSNs, its surface is commonly functionalised by various suitable chemical groups. These proper chemical groups have the capability to link with the drug molecules via strong bonds. Consequently, all-encompassing attempts have been made toward the functionalisation of MSNs. Diverse strategies such as post-synthesis grafting, co-condensation, and post-polymerisation have been successfully achieved and reported [14].

The modification by the co-condensation method and post-synthetic grafting process authorise us to selectively modify the exterior and interior surface of MSNs with the desired functional groups, which is suitable for applications in areas such as catalysis, drug delivery, sorption, separation and sensors [15–17].

The post-polymerisation method has been less investigated on DDSs. In this method, mesoporous polymer–inorganic hybrid materials are prepared via in situ free radical polymerisation of vinyl-based monomers, which are cramped at the mesopore surface. Upon polymerisation of the monomers, in the inner pores of the MSNs, a thin layer of a polymer is generated, whereas the mesopores remained entirely available. This method gives an opportunity to transfer the desirable physical properties of the MSNs such as ordered mesostructure and large pore diameter. In addition, it makes it possible to introduce various functional groups [18].

The poly(acrylic acid) (PAA) polymer is a well-known bio-adhesive hydrogel that can shield some protein drugs from degradation, jabbing to the mucosal lining of the upper small intestine. The PAA is carrying carboxylic moieties, which are able to release hydrogen at both low and high pH [19]. Subsequently, the PAA cannot act lonely as a smart uptake and release system. Thus, the PAA should be modified by other compounds. Adding cross-linked compounds is one of the best methods to fortify polymers. Thanks to this method, some properties of the polymer such as solubility and collapsing in different pHs can be changed [19, 20]. Therefore, the successful control of uptake and release of drugs is achieved.

Herein, we wish to introduce a simple, but highly efficient polymer–silica nanocomposite carrier system based on a cage-type mesoporous silica with a three-dimensional (3D) porous network (KIT-6) and poly(AA) acting as a biocompatible hydrogel. In addition, ethylene glycol dimethacrylate (EGDMA) was used as a cross-linking agent. The potency of the nanocomposite [KIT-6/Poly(AA-EGDMA)] to load drug molecules was studied. In this investigation, we used the prescribed drug, ibuprofen (IBU) as a model drug. The release pattern was examined in a simulated body fluid (SBF). For evaluation of the competence and efficiency of the carrier system, a comparison was made using pure KIT-6 as a vehicle. Thanks to these amendments, drugs are released in response to changes in the polarity of the environment with exact controlling.

2. Experimental

2.1. Main materials: Pluronic P123 (EO20PO70EO20) was provided by Sigma-Aldrich. AA as a monomer was purchased from Kimiyagaran Emrooz Co. Tetraethylorthosilicate (TEOS), hydrochloric acid (37 wt% HCl), *n*-butanol, EGDMA, ammonium peroxodisulphate as an initiator and other chemicals were bought from Merck Co. (Darmstadt, Germany).

2.2. Characterisation of samples: The samples were identified using Fourier transform infrared spectroscopy (FTIR) (a Perkin Elmer 65 in a KBr tablet in the 4000–400 cm^{-1} limited area).The BEL SORP 18 series used for the determination of Brunauer–Emmett–Teller (BET)-specific surface areas and Barrett-Joyner-Halenda (BJH) pore size distribution of the samples by adsorption– desorption of nitrogen at the liquid nitrogen temperature. The X-ray powder diffraction (XRD) of the samples was performed using a Bruker D8 Advance X-ray employing nickel-filtered Cu Ka radiation. Data analysis of the thermal gravimetric analysis (TGA) in a temperature range of 30–450°C was performed by using a Perkin-Elmer TG (STA-6000).

2.3. Sample preparation

2.3.1. Synthesis of KIT-6: The 3D porous network (KIT-6) was prepared following the method previously, reported by Ryoo [21]. In this procedure, 6 g (1.03 mmol) of P123 and 6 g of *n*-butanol (0.161 mol) were dissolved in 270 g (15 mol) of deionised water and 11.4 g (0.115 mol) of concentrated hydrochloric acid (37 wt% HCl). Then, 12.9 g (0.061 mol) of TEOS was added to this mixture. For 24 h, the mixture was stirred at 45°C during which a mesostructured product was formed. After that, the reaction mixture was heated at 95°C for 24 h. The solid product was filtered. Then washed with distilled water and dried at 100°C. Finally, the samples were calcined at 550°C for 6 h to remove the template.

2.3.2. Preparation of KIT-6/poly(AA-EGDMA) nanocomposites: In a typical procedure, 0.5 g KIT-6 and 0.25 g, AA in 5 mL of deionised water was deposited in a round bottom flask and the mixture was stirred for 24 h at room temperature to allow monomers merge in KIT-6 pores. Then, 0.024 g ammonium persulphate as an initiator and 0.034 g ethylene glycol dimethacrylate (EGDMA) as a cross-linking agent were added, and the temperature of the mixture was increased to 75°C gradually, then kept fixed for 5 h while being stirred under N_2 gas. The resulting white powder nanocomposite [KIT-6/Poly(AA-EGDMA)] was filtrated, washed with acetone several times, and finally dried at 80°C overnight (Fig. 1).

2.3.3. Drug loading: The IBU loading process was investigated on the KIT-6, the modified nanocomposites KIT-6/Poly (AA-EGDMA) and Poly(AA-EGDMA). According to the previous research, *n*-hexane as a solvent with more solubility capacity for IBU was chosen to load IBU on the carriers [22].

For investigation of drugs' loading, 20 mL of IBU solution (20 mg L^{-1}, 2.0 g IBU in 100 ml n-hexane) was blended with 0.4 g of KIT-6 (ratio of KIT-6: IBU, 1:1) in a closed container. The mixed solution was shaken at 200 rpm for 48 h at 25°C. Then, the mixture was filtered and the supernatant was diluted by *n*-hexane to obtain the drug concentration by using an ultraviolet (UV)-visible spectrophotometer at 272 nm. The drug loading processes were repeated three times.

2.3.4. Drug release investigation: The study of the *in vitro* drug release from KIT-6, Poly(AA-EGDMA), and KIT-6/Poly (AA-EGDMA) was conducted by soaking a carrier loaded IBU in 50 mL of SBF with pH 7.4 without shaking at 37°C. UV-vis spectrometry was used as an analytical method at 272 nm to measure the amount of IBU released as a subsidiary of time. To investigate the reproducibility, the process was repeated three times.

3. Results and discussion

3.1. Characterisation of KIT-6/Poly(AA-EGDMA): Fig. 2 shows the FTIR spectra of KIT-6, poly(AA-EGDMA), and KIT-6/Poly(AA-EGDMA).

The bands at 1080, 817, and 470 cm^{-1} are related to Si–O–Si asymmetrical stretching vibration, symmetrical stretching vibration and bending vibration, respectively, which are related to KIT-6 and KIT-6/Poly(AA-EGDMA) [23]. In addition, the FTIR of KIT-6 shows the band around 945–957 cm^{-1}, which is assigned to Si–OH vibrations of silanols in the surface that refer to the characteristics of mesoporous silica [23]. The FTIR spectrum of KIT-6 contains the broad band around 3448 cm^{-1} which is assigned to the O–H stretching of water. Also, the hydroxyl stretching of hydrogen bonded internal silanol groups appears in this range. The peak at 1635 cm^{-1} corresponds to the bending mode of OH of water [23]. The FTIR spectrum of AA-copolymer (poly-(AA-EGDMA)) contains the peak at 1726 cm^{-1} that is related to the (C=O) bond stretching vibration of the carbonyl group of AA [22]. It can be seen that the absorption peak at 1616 cm^{-1} corresponds to the C=C bond in AA and disappears after polymerisation [24]. The KIT-6/Poly(AA-EGDMA) shows several peaks around 2800–3000 cm^{-1} that correspond to the aliphatic C–H stretching. The appearance of the above bands could prove that AA is attached to the Si–OH group of KIT-6 and that the KIT-6/Poly (AA-EGDMA) has been obtained.

The XRD patterns of KIT-6 and KIT-6/Poly(AA-EGDMA) are shown in Fig. 3. The XRD pattern of KIT-6 should have peaks related to 3D cubic symmetry (Ia3d).

As is seen one sharp peak at 2θ about 0.95 and two weak peaks at 2θ about 1.65 and 1.9, which can be indexed as (211), (220), and (320) reflections that proved this type of structure [14, 15]. The

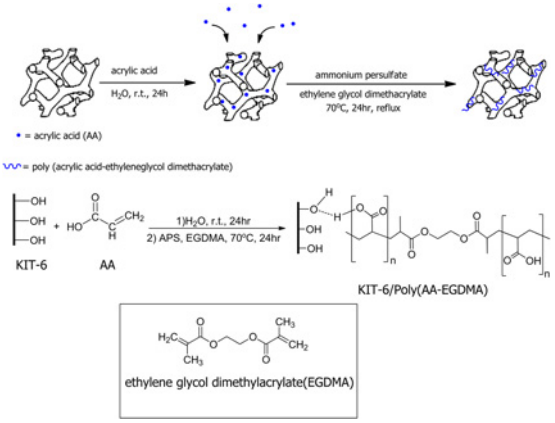

Fig. 1 *Schematic formation process of KIT-6/Poly(AA-EGDMA)*

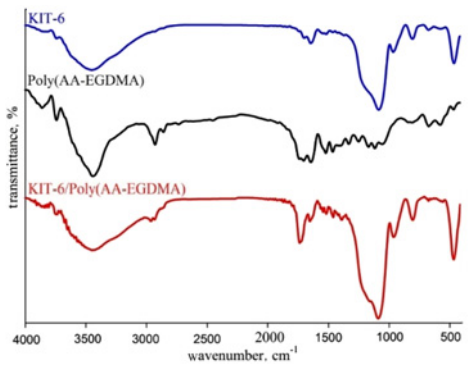

Fig. 2 *FTIR spectra of KIT-6, Poly(AA-EGDMA) and KIT-6/Poly (AA-EGDMA)*

doi: 10.1049/mnl.2017.0451

XRD pattern of KIT-6/Poly(AA-EGDMA) ($2\theta = 0.6$–10) exhibits the same type of structural pattern of the KIT-6 (211); however, the intensity of the characteristic reflection peaks of the KIT-6/Poly(AA-EGDMA) ($2\theta = 0.6$–10) is weaker than the XRD pattern of KIT-6. The intensity reduction of characteristic reflection peaks may be related to the symmetry reduced via the hybridisation of KIT-6, which is also found in the ordered mesoporous silica loaded with organic groups [18, 23]. In addition, the content reduction of the siliceous material by poly(AA-EGDMA) can also be effective in a decrease in peak intensity.

In Fig. 4, the N_2 adsorption/desorption isotherms of KIT-6 and KIT-6/Poly(AA-EGDMA) nanocomposites are displayed.

Both samples show the isotherms of type IV with a H1 type hysteresis loop and a sharp capillary condensation step in the 0.5–0.9 P/P_0 range, which are the typical feature of large channel-like porous materials with a narrow range pore-size distribution [25].

The specific surface area, total pore volume and pore sizes of KIT-6 and KIT-6/Poly(AA-EGDMA) were calculated by using BET and BJH methods. The information obtained is summarised in Table 1. After hybridisation with Poly(AA-EGDMA), KIT-6/Poly(AA-EGDMA) exhibits a smaller specific surface area, pore size, and pore volume than pure KIT-6, which is probably because of the polymer existing in the mesopores of KIT-6 (Table 1).

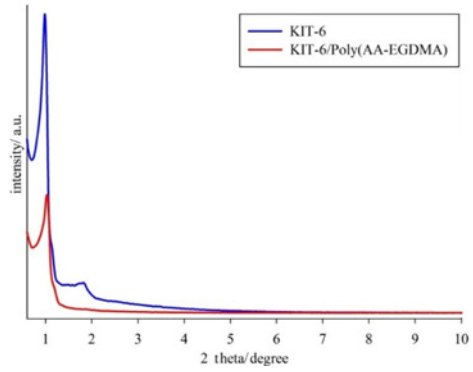

Fig. 3 *Powder XRD patterns of KIT-6 and KIT-6/Poly(AA-EGDMA)*

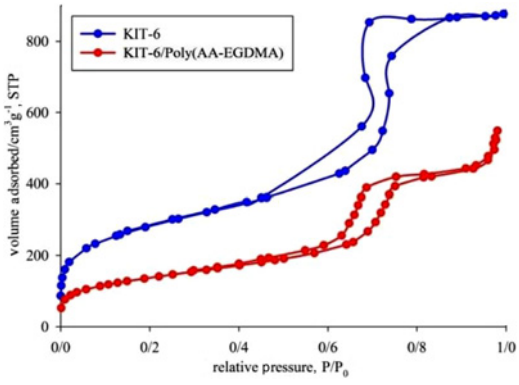

Fig. 4 *N_2 adsorption–desorption isotherms of KIT-6 and KIT-6/Poly (AA-EGDMA)*

Moreover, the corresponding pore size distribution curves of KIT-6 and KIT-6/Poly(AA-EGDMA) are plotted in Fig. 5, which shows a narrow distribution with 8 and 6 nm pore diameter, respectively. According to the results, the carrier retains a mesoporous form with a sufficient surface area (488 $m^2\ g^{-1}$).

Fig. 6 presents the TGA curves of KIT-6 and KIT-6/Poly (AA-EGDMA) under a nitrogen atmosphere. The TG curve of KIT-6 shows a mass loss around ~80°C (6.58%, w/w), which may be related to the evaporation of water from KIT-6 surfaces. According to the TG curve, KIT-6 has excellent thermal stability at temperatures ranging from 100 to 500°C and no degradation or mass loss can be seen.

The TGA curve of KIT-6/Poly(AA-EGDMA) consists of three steps of mass loss. A small mass loss (around 5.5%, w/w) at 100°C is dependent on adsorbed water that exists in the mesopores of KIT-6. At a temperature around 250°C, the KIT-6/Poly (AA-EGDMA) shows a stage of degradation. The mass loss of KIT-6/Poly(AA-EGDMA) in the second step is equal to 4.13% (w/w), which can be related to the partial destruction of polymer chains. The third stage of weight loss that occurred at 423°C is related to the main degradation of polymer chains (around 13%, w/w) [26].

As shown in Fig. 7, the surface morphologies of the obtained KIT-6 and KIT-6/Poly(AA-EGDMA) were inspected by the SEM technique. KIT-6 and KIT-6/Poly(AA-EGDMA) are aggregates of tiny atypical particles with a relatively smooth surface.

Almost no striking difference is observed in surface morphology between KIT-6 and KIT-6/Poly(AA-EGDMA) nanocomposites, which indicates that probably the polymerisation of Poly(AA-EGDMA) was situated more inside the pores of KIT-6 than the outside surfaces [23].

3.2. Application of KIT-6/poly(AA-EGDMA) as an IBU carrier: As stated before, IBU loading was performed by soaking different matrices in IBU in *n*-hexane solution for 48 h at room temperature. The amount of absorbed IBU was measured by using an UV-Vis spectrophotometer in one of the λ_{max} of the IBU wavelength, at 272 nm. The initial and final concentrations of IBU solutions were determined by measuring the UV-visible spectrum. The loading percentage was calculated according to the following equation:

$$\%\text{loading} = \frac{\text{weight of loaded drug}}{\text{initial weight of drug}} \times 100, \quad (1)$$

where the weight of loaded drug = initial weight of drug – weight of drug remaining after 48 h of loading.

3.2.1. Characterisation of KIT-6/Poly(AA-EGDMA) loaded with IBU (IBU/KIT-6/Poly(AA-EGDMA)): Fig. 8 shows the FTIR spectra that verify the interaction of IBU with KIT-6/Poly(AA-EGDMA).

The pure IBU spectrum exhibits the characteristic peaks at around 2954 and 2871 cm^{-1} related to C–H stretching vibrations from the alkyl group of IBU molecules and the sharp peak at 1719 cm^{-1} defines the carboxylic group of IBU. The FTIR of IBU/KIT-6/Poly(AA-EGDMA) displays the characteristics of both silica (see Fig. 2) and IBU, confirming that IBU is successfully loaded into the pores of KIT-6/Poly(AA-EGDMA). In addition, the

Table 1 Physicochemical properties of KIT-6 and KIT-6/Poly(AA-EGDMA) samples obtained from N_2 adsorption

Sample	$S_{mesopore}$, $m^2\ g^{-1a}$	$V_{mesopore}$, $cm^3\ g^{-1a}$	$D_{mesopore}$, nm[a]	$S_{mesopore}$, $m^2\ g^{-1b}$	$V_{mesopore}$, $cm^3\ g^{-1b}$	$D_{mesopore}$, nm[b]
KIT-6	989	1.35	8.5	761	1.2	8
KIT-6/Poly(AA-EGDMA)	488	0.85	7	422	0.8	6.2

[a]Calculated by the BET method.
[b]Calculated by the BJH method.

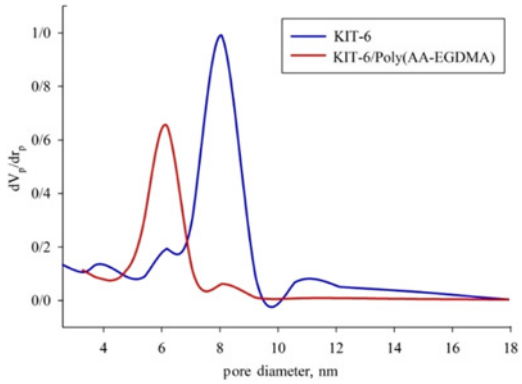

Fig. 5 *Pore size distributions of KIT-6 and KIT-6/Poly(AA-EGDMA)*

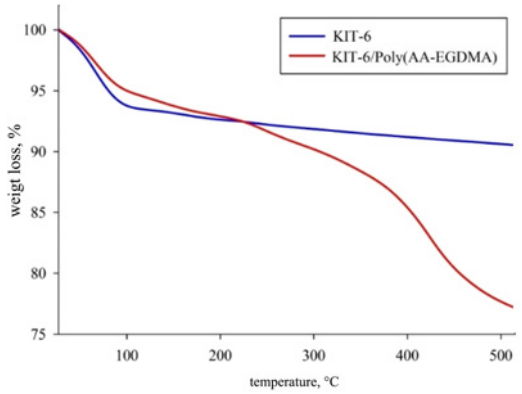

Fig. 6 *TGA curve of KIT-6 and KIT-6/Poly(AA-EGDMA)*

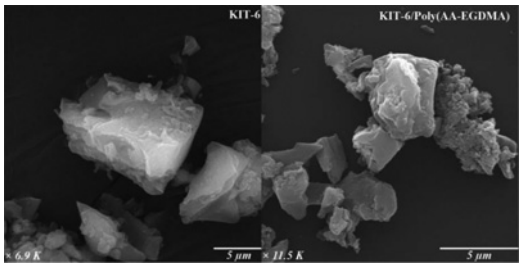

Fig. 7 *Scanning electron microscopy (SEM) photographs of KIT-6 and KIT-6/Poly(AA-EGDMA)*

shoulder at 965 cm^{-1}, which represents the existence of residual silanol groups, almost disappears after IBU loading. This fact indicates the formation of a hydrogen bond between the carboxylic group of IBU and the silanol groups on the silica surface [27–29].

Fig. 9 shows the SEM images of IBU/KIT-6/Poly(AA-EGDMA) with ×6900 and ×7700 magnification. By comparing the image obtained from the IBU/KIT-6/Poly(AA-EGDMA) with the pure KIT-6 (Fig. 7), no serious changes are observed in the nanocomposite morphology after drug loading.

This result confirms that most of the IBU is immobilised into the pores of the nanocomposite. However, some of it is immobilised on the outer surface of the nanocomposite, which is responsible for the fast drug release in the first step of release.

3.2.2. Loading of IBU and release study: The method of one-factor at a time was used to study the optimum conditions of drug loading. Several factors like drug loading process time and the weight ratio of drug molecules to the matrix were investigated. As seen in Table 2, outcomes show that the time factor causes an increase in loading the drug on the surface of KIT-6 to some extent (17% loading IBU in 48 h). Therefore, 48 h was chosen as a modified time of drug loading.

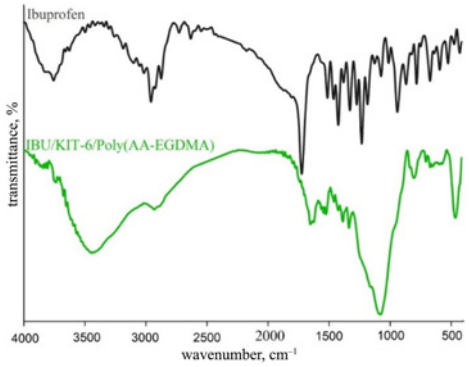

Fig. 8 *FTIR spectra of IBU and IBU/KIT-6/Poly(AA-EGDMA)*

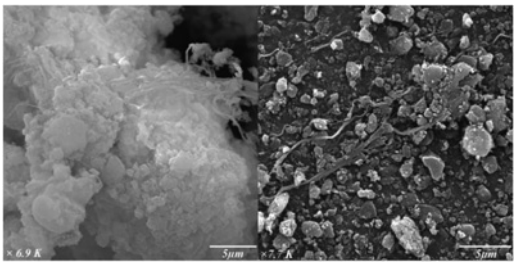

Fig. 9 *SEM photographs of IBU/KIT-6/Poly(AA-EGDMA)*

Table 2 Effect of drug loading process time on the adsorption of IBU on KIT-6

Time of drug loading, h	24	48	72
Drug loading on KIT-6, %	15	17	17.5

At the next step, the weight ratio of drug molecules to different matrices including KIT-6, Poly(AA-EGDMA), and KIT-6/Poly (AA-EGDMA) under the same conditions (2.3.3 section) was studied, and the results are shown in Fig. 10. To increase the weight of the drug to the carrier, the concentration of the drug sol ution was kept constant and the volume of the IBU solution (20 mg L^{-1}, 2.0 g IBU in 100 ml *n*-hexane) to the matrix was increased.

As can be seen, the amounts of IBU loaded into the KIT-6 were less than both Poly(AA-EGDMA) and KIT-6/Poly(AA-EGDMA) (19, 35 and 29% drug loading, respectively). Actually, inadequate interaction (forming hydrogen bonding) between silanol groups and carboxylic acid groups of IBU can interpret this result. In addition, the drug uptake of KIT-6/Poly(AA-EGDMA) is slightly lower than Poly(AA-EGDMA). Substantially, in the case of KIT-6/Poly(AA-EGDMA), some of the carboxylic acid groups of poly(AA) are bonded to the silanol groups of KIT-6 by hydrogen bonding, and subsequently, the number of accessible carboxylic groups of the polymer is limited. Moreover, the amounts of the polymer are alleviated by diluting it with KIT-6, which affects the total hydrogen bond formed between the carboxylic groups of the polymer and carboxylic acid groups of IBU. Therefore, the lower amount of drug uptake by KIT-6/Poly(AA-EGDMA) than Poly(AA-EGDMA) is reasonable. The results illustrate that by increasing the weight ratio of the amount of IBU to KIT-6/Poly (AA-EGDMA) (from 17% for 1:1, to 29% for 3:1, the weight ratio of IBU to the matrix), the IBU loading increases. Then, by increasing the weight ratio of the amount of IBU to nanocomposite (30% drug loading for 4:1 and 5:1 ratios) more, the amount of loaded IBU remains constant (Fig. 10).

doi: 10.1049/mnl.2017.0451

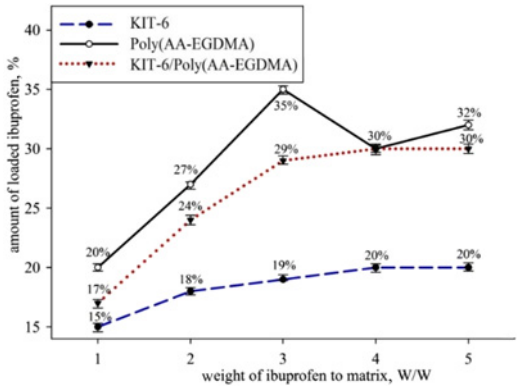

Fig. 10 *IBU loading profile on different matrices KIT-6, Poly (AA-EGDMA), and KIT-6/Poly(AA-EGDMA)*

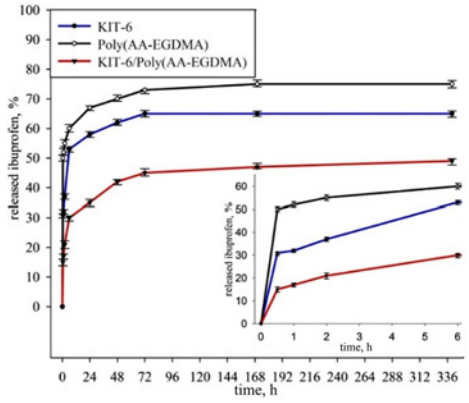

Fig. 11 *Profile of IBU release from various carriers KIT-6, Poly (AA-EGDMA), and KIT-6/Poly(AA-EGDMA)*

Therefore, a 3:1 weight ratio of IBU to nanocomposite with 29% (w/w) drug loading to the matrix was determined as an optimum scale. In the case of Poly(AA-EGDMA), which accounts for being heterogeneous polymeric chains, erratic loading of the IBU pattern is shown (Fig. 10). Actually, as we know, polymerisation in the bulk is not a uniform and controllable process and it can be expected that we will have polymers with various molecular weights and shapes. Therefore, irregular drug uptake and release in these systems would be expected (in this study we observed the irregular drug loading by increasing the weight ratio of the amount of IBU to nanocomposite, 35% for 3:1 and 30% for 4:1). Whereas, in the case of KIT-6/Poly(AA-EGDMA), which is prepared by in situ polymerisation of AA monomers inside the pores of KIT-6, polymerisation is more controllable because there is not enough space for the growth of polymer chains inside the pores. In this case, the polymerisation is more uniform (narrow pore size distribution of KIT-6/Poly(AA-EGDMA) obtained from the N_2 adsorption–desorption analysis (BJH method), which proves this idea, and KIT-6/Poly(AA-EGDMA) shows regular drug uptake and release. It is an important issue for drug delivery carriers.

For investigation of drug release, evaluation was based on Section 2.3.4. The absorbance spectrum in λ_{max} at 272 nm was used for monitoring the release amount as a function of time, and the release percentage was calculated according to the following equation:

$$\%\text{Release} = \frac{\text{weight of drug in solution}}{\text{weight of drug in carrier}} \times 100. \qquad (2)$$

Spectrophotometric analysis of the SBF supernatant of different matrices achieved information about the release pattern of the carrier. As shown in Fig. 11, the initial burst of IBU release illustrates a cumulative release profile in all samples [10, 30 and 50% drug release for KIT-6/Poly(AA-EGDMA), KIT-6 and Poly (AA-EGDMA), respectively]. It could be due to the IBU adsorbed on the outer surface of the KIT-6, Poly(AA-EGDMA), and KIT-6/Poly(AA-EGDMA) that can be easily released into the aquatic environment.

Careful investigations on releasing IBU from KIT-6 demonstrate that the pattern of drug release is faster than that of KIT-6/Poly (AA-EGDMA) (50% released of drug loading at 6 h for KIT-6, versus 29% released for KIT-6/Poly(AA-EGDMA)), which belongs to the drugs adsorbed on the outer surfaces of KIT-6. After that, for the drugs, which are incorporated inside the pores of KIT-6, the bi-continuous cubic mesostructures of KIT-6 by Ia3d symmetry and the interpenetrating cylindrical pore system do not allow the drugs to be released in full [30] (Fig. 12*a*). The major reason IBU can be released from KIT-6 is hydrogen bonding, which is created between water and IBU [31].

According to Fig. 11, the amount of drug released from Poly (AA-EGDMA) is far more than that released from KIT-6/Poly (AA-EGDMA) (60 and 29% release of drug loading, respectively

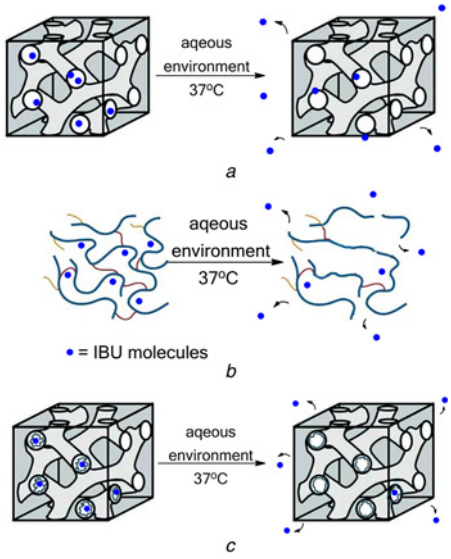

Fig. 12 *Schematic release process of IBU molecules from*
a KIT-6
b Poly(AA-EGDMA)
c KIT-6/Poly(AA-EGDMA)

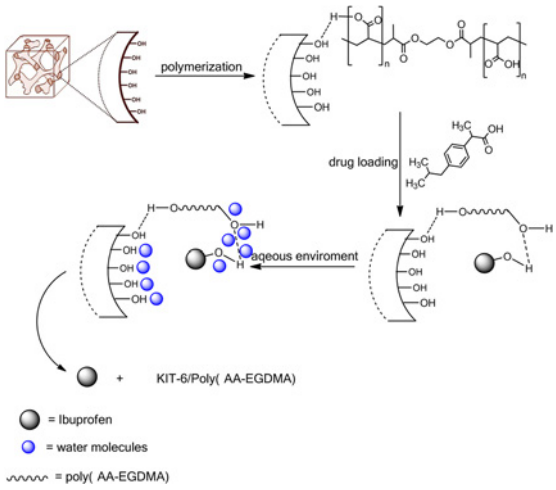

Fig. 13 *Proposed mechanism of drug release from the nanocomposite*

in 6 h). As the hydrogen bond forming between IBU and water is stronger than that of bond forming between the carboxyl groups of the polymer and IBU, the drug is released from the surface of Poly(AA-EGDMA) (Fig. 13).

Moreover, there is another factor to control the releasing of the drug from Poly(AA-EGDMA). As we know, poly(AA) is a hydrogel with a hydrophilic nature. By adsorbing water in aqueous circumstances, polymer branches of the hydrogel are expanded, and encapsulated drugs can be released easily (Fig. 12*b*). Consequently, large amounts of the drug are released in earlier times in the case of Poly(AA-EGDMA).

In the case of KIT-6/Poly(AA-EGDMA), the polymer chains, which are formed in the pores of KIT-6, will trap the drug molecules by hydrogen bonding. In the SBF media, the polymer chains held in the pores cannot easily absorb water and the swelling process is done slowly and is controllable. Therefore, the release of the drug from KIT-6/Poly(AA-EGDMA) occurs more slowly and is controllable (Fig. 12*c*).

4. Conclusion: To introduce a smart uptake and release carrier system, a KIT-6/Poly(AA-EGDMA) nanocomposite, based on highly ordered large pore mesoporous silica molecular sieves, has been prepared by a simple method. KIT-6 with bi-continuous cubic mesostructures of Ia3d symmetry and an interpenetrating cylindrical pore system could be a good choice to be used in sustained release and drug delivery. The results of loading and releasing of IBU indicated that the KIT-6/Poly(AA-EGDMA) can be used as a high potential drug carrier because the polymer chains of AA, as a hydrogel polymer, as well as a regular network structure of mesoporous kit-6, can have a significant effect on the drug-release control. Moreover, poly(AA) has several perfect characteristics such as non-toxicity, hydrophilic nature, hydrogel properties and high interaction with a drug, which make it a trapping drug agent. Moreover, because the amount of drug and polymer loaded into KIT-6 is substantial, the optimising circumstance is fundamental, as attained in this investigation.

5. Acknowledgment: The authors are thankful to the Alzahra University Research Council. MMH is also thankful for financial supports given by individual research chair granted by INSF.

6 References

[1] Lee J.H., Yeo Y.: 'Controlled drug release from pharmaceutical nano carriers', *Chem. Eng. Sci.*, 2015, **125**, pp. 75–84
[2] Zhang X., Li F., Guo S., *ET AL.*: 'Biofunctionalized polymer-lipid supported mesoporous silica nanoparticles for release of chemotherapeutics in multidrug resistant cancer cells', *Biomaterials*, 2014, **35**, pp. 3650–3665
[3] Lian H.-Y., Hu M., Liu C.-H., *ET AL.*: 'Highly biocompatible, hollow coordination polymer nanoparticles as cisplatin carriers for efficient intracellular drug delivery', *Chem. Commun.*, 2012, **48**, pp. 5151–5153
[4] Shieh F.-K., Wang S.-C., Yen C.-I., *ET AL.*: 'Imparting functionality to biocatalysts via embedding enzymes into nanoporous materials by a de novo approach: size-selective sheltering of catalase in metal–organic framework microcrystals', *J. Am. Chem. Soc.*, 2015, **137**, pp. 4276–4279
[5] Liang Y.-H., Liu C.-H., Liao S.-H., *ET AL.*: 'Cosynthesis of cargo-loaded hydroxyapatite/alginate core-shell nanoparticles (HAP@Alg) as pH-responsive nanovehicles by a pregel method', *Appl. Mater. Interfaces*, 2012, **4**, pp. 6720–6727
[6] Bastakoti B.P., Hsu Y.-C., Liao S.-H., *ET AL.*: 'Inorganic–organic hybrid nanoparticles with biocompatible calcium phosphate thin shells for fluorescence enhancement', *Chem. Asian J.*, 2013, **8**, pp. 1301–1305
[7] Zhang Y., Wang Z., Zhou W., *ET AL.*: 'Cationic poly(ε-caprolactone) surface functionalized mesoporous silica nanoparticles and their application in drug delivery', *Appl. Surf. Sci.*, 2013, **276**, pp. 769–775
[8] Tang H., Guo J., Sun Y., *ET AL.*: 'Facile synthesis of pH sensitive polymer-coated mesoporous silica nanoparticles and their application in drug delivery', *Int. J. Pharm.*, 2011, **421**, pp. 388–396
[9] Jia L., Shen J., Li Z., *ET AL.*: 'In vitro and in vivo evaluation of paclitaxel-loaded mesoporous silica nanoparticles with three pore sizes', *Int. J. Pharm.*, 2013, **445**, pp. 12–19
[10] Zheng Q., Lin T., Wu H., *ET AL.*: 'Mussel-inspired poly dopamine coated mesoporous silica nanoparticles as pH-sensitive nano carriers for controlled release', *Int. J. Pharm.*, 2014, **463**, pp. 22–26
[11] Ho J., Huang Y., Danquah M.K., *ET AL.*: 'Synthesis of biodegradable polymer–mesoporous silica composite microspheres for DNA prime-protein boost vaccination', *Eur. J. Pharm. Sci.*, 2010, **39**, pp. 412–420
[12] Mamaeva V., Sahlgren C., Lindén M.: 'Mesoporous silica nanoparticles in medicine-recent advances', *Adv. Drug Deliv. Rev.*, 2013, **65**, pp. 689–702
[13] Yu F., Tang X., Pei M.: 'Facile synthesis of PDMAEMA-coated hollow mesoporous silica nanoparticles and their pH-responsive controlled release', *Microporous Mesoporous Mater.*, 2013, **173**, pp. 64–69
[14] Xiea M., Shi H., Lia Z., *ET AL.*: 'A multifunctional mesoporous silica nanocomposite for targeted delivery, controlled release of doxorubicin and bioimaging', *Colloids Surf. B, Biointerfaces*, 2013, **110**, pp. 138–147
[15] Dutta S., Bhaumik A., Wu K.C.-W.: 'Hierarchically porous carbon derived from polymers and biomass: effect of interconnected pores on energy applications', *Energy Environ. Sci.*, 2014, **7**, (11), pp. 3574–3592
[16] Hsu S.-H., Li C.-T., Chien H.-T., *ET AL.*: 'Platinum-free counter electrode comprised of metal–organic-framework (MOF)-derived cobalt sulfide nanoparticles for efficient dye-sensitized solar cells (DSSCs)', *Sci. Rep.*, 2014, **4**, Article number: 6983
[17] Lee Y.-C., Dutta S., Wu K.C.-W.: 'Integrated, cascading enzyme-/chemocatalytic cellulose conversion using catalysts based mesoporous silica nanoparticles', *ChemSusChem*, 2014, **7**, pp. 3241–3246
[18] Tian B., Yang C.: 'Thermo-sensitive poly(*N*-isopropylacrylamide)/mesoporous silica nanocomposites as controlled delivery carriers: loading and release behaviors for drug ibuprofen', *J. Nanosci. Nanotechnol.*, 2011, **11**, (3), pp. 1871–1879
[19] Hong C.-Y., Li X., Pan C.-Y.: 'Fabrication of smart nanocontainers with a mesoporous core and a pH-responsive shell for controlled uptake and release', *J. Mater. Chem. A*, 2009, **19**, pp. 5155–5160
[20] Jin S., Liu M., Chen S., *ET AL.*: 'A drug-loaded gel based on polyelectrolyte complexes of poly (acrylic acid) with poly(vinylpyrrolidone) and chitosan', *Mater. Chem. Phys.*, 2010, **123**, pp. 463–470
[21] Kleitz F., Choi S.H., Ryoo R.: 'Cubic Ia3d large mesoporous silica: synthesis and replication to platinum nanowires, carbon nanorods and carbon nanotubes', *Chem. Commun.*, 2003, **17**, pp. 2136–2137
[22] Kalbasi R.J., Zirakbash A.: 'Synthesis, characterization and drug release studies of poly(2-hydroxyethyl methacrylate)/KIT-5 nanocomposite as an innovative organic–inorganic hybrid carrier system', *RSC Adv.*, 2015, **5**, pp. 12463–12471
[23] Kalbasi R.J., Mosaddegh N.: 'Palladium nanoparticles supported on poly(2-hydroxyethyl methacrylate)/KIT-6 composite as an efficient and reusable catalyst for Suzuki–Miyaura reaction in water', *J. Inorg. Organomet. Polym. Mater.*, 2012, **22**, pp. 404–414
[24] Amin M.C.I.M., Ahmad N., Halib N., *ET AL.*: 'Synthesis and characterization of thermo- and pH-responsive bacterial cellulose/acrylic acid hydrogels for drug delivery', *Carbohydr. Polym.*, 2012, **88**, pp. 465–473
[25] Teng Y., Wu X., Zhou Q., *ET AL.*: 'Direct electron transfer of myoglobin in mesoporous silica KIT-6 modified on screen-printed electrode', *Sens. Actuators B, Chem.*, 2009, **142**, pp. 267–272
[26] Lungu A., Perrin F.X., Belec L., *ET AL.*: 'Kaolin/poly(acrylic acid) composites as precursors for porous kaolin ceramics', *Appl. Clay Sci.*, 2012, **62-63**, pp. 63–69
[27] Ghaeni Panah N., Alizadeh P., Eftekhari Yekta B., *ET AL.*: 'Preparation and in-vitro characterization of electrospun bioactive glass nano tubes as mesoporous carriers for ibuprofen', *Ceram. Int.*, 2016, **42**, pp. 10935–10942
[28] Bian Z., Tang J., Hu J., *ET AL.*: 'Controlled-release of ibuprofen on multilayer mesoporous vesicle', *Colloids Surf. A: Physicochem. Eng. Aspects*, 2013, **436**, pp. 1021–1026
[29] Gao L., Sun J., Zhang L., *ET AL.*: 'Influence of different structured channels of mesoporous silicate on the controlled ibuprofen delivery', *Mater. Chem. Phys.*, 2012, **135**, pp. 786–797
[30] Ayad M.M., Salahuddin N.A., Abu El-Nasr A., *ET AL.*: 'Amine-functionalized mesoporous silica KIT-6 as a controlled release drug delivery carrier', *Microporous Mesoporous Mater.*, 2016, **229**, pp. 166–177
[31] Wang W., Qi R., Shan W., *ET AL.*: 'Synthesis of KIT-6 type mesoporous silicas with tunable pore sizes, wall thickness and particle sizes via the partitioned cooperative self-assembly process', *Microporous Mesoporous Mater.*, 2014, **194**, pp. 167–173

doi: 10.1049/mnl.2017.0451